Short Communication

Prediction of dynamic friction forces in spur gears using alternate sliding friction formulations

Song He, Sungmin Cho, Rajendra Singh*

Acoustics and Dynamics Laboratory, Department of Mechanical Engineering and Center for Automotive Research, The Ohio State University, Columbus, OH 43210, USA

Abstract

In this communication, several sliding friction formulations used in spur gear dynamics are examined and compared in terms of the predictions of interfacial friction forces and off-line-of-action motions. Competing friction formulations include Coulomb models with time-varying friction coefficients and empirical expressions based on elasto-hydrodynamic and/or boundary lubrication regime principles. Predicted results compare well with friction force measurements.
© 2007 Elsevier Ltd. All rights reserved.

1. Introduction

Gear dynamic researchers [1–7] have typically modeled sliding friction phenomenon by assuming Coulomb formulation with a constant coefficient (μ) of friction (it is designated as Model I in this communication). In reality, tribological conditions change continuously due to varying mesh properties and lubricant film thickness as the gears roll through a full cycle [8–11]. Thus, μ varies instantaneously with the spatial position of each tooth and the direction of friction force changes at the pitch point. Alternative tribological theories, such as elasto-hydrodynamic lubrication (EHL), boundary lubrication or mixed regime, have been employed to explain the interfacial friction in gears [8–11]. For instance, Benedict and Kelley [8] proposed an empirical dynamic friction coefficient (designated as Model II) under mixed lubrication regime based on measurements on a roller test machine. Xu et al. [9,10] recently proposed yet another friction formula (designated as Model III) that is obtained by using a non-Newtonian, thermal EHL formulation. Duan and Singh [12] developed a smoothened Coulomb model for dry friction in torsional dampers; it could be applied to gears to obtain a smooth transition at the pitch point and we designate this as Model IV. Hamrock and Dawson [11] suggested an empirical equation to predict the minimum film thickness for two disks in line contact. They calculated the film parameter Λ, which could lead to a composite, mixed lubrication model for gears (designated as Model V). Overall, no prior work has incorporated either the time-varying $\mu(t)$ or Models II to V, into multi-degree-of-freedom (MDOF) gear dynamics. To overcome this void in the literature, specific objectives of this communication are established as follows: (1) propose an improved MDOF spur gear pair model with

---

*Corresponding author. Tel.: +1 614 292 9044; fax: +1 614 292 3163.

E-mail address: singh.3@osu.edu (R. Singh).

time-varying coefficient of friction, $\mu(t)$, given realistic mesh stiffness profiles [4]; (2) comparatively evaluate alternate sliding friction models and predict the interfacial friction forces and motions in the off-line-of-action (OLOA) direction; and (3) validate one particular model (III) by comparing predictions to the benchmark gear friction force measurements made by Rebbechi et al. [13].

2. MDOF spur gear model

Transitions in key meshing events within a mesh cycle are determined from the undeformed gear geometry. Fig. 1(a) is a snapshot for the example gear set (with a contact ratio σ of about 1.6) at the beginning ($t = 0$) of the mesh cycle (t_c). At that time, pair ♯1 (defined as the tooth pair rolling along line AC) just comes into mesh at point A and pair ♯0 (defined as the tooth pair rolling along line CD) is in contact at point C, which is the highest point of single tooth contact (HPSTC). When pair ♯1 approaches the lowest point of single tooth contact (LPSTC) at point B, pair ♯0 leaves contact. Further, when pair ♯1 passes through the pitch point P, the relative sliding velocity of the pinion with respect to the gear is reversed, resulting in a reversal of the friction force. Beyond point C, pair ♯1 will be re-defined as pair ♯0 and the incoming meshing tooth pair at point A will be re-defined as pair ♯1, resulting in a linear time-varying (LTV) formulation. The spur gear system model is shown in Fig. 1(b) and key assumptions for the dynamic analysis include the following: (i) pinion and gear are rigid disks; (ii) shaft-bearing stiffness elements in the line-of-action (LOA) and OLOA directions are modeled as lumped springs which are connected to a rigid casing; (iii) vibratory angular motions are small in comparison to the kinematic motion. Overall, we obtain a linear time-varying system formulation, as explained in the previous paper [4] with a constant μ. Refinements to the multi-degree-of-freedom model of Fig. 1 with time-varying sliding friction $\mu(t)$ are proposed as follows. The governing equations for the torsional motions $\theta_p(t)$ and $\theta_g(t)$ are as follows:

$$J_p \ddot{\theta}_p(t) = T_p + \sum_{i=0}^{n=\text{floor}(\sigma)} X_{pi}(t) F_{pfi}(t) - \sum_{i=0}^{n=\text{floor}(\sigma)} r_{bp} N_{pi}(t), \tag{1}$$

$$J_g \ddot{\theta}_g(t) = -T_g + \sum_{i=0}^{n=\text{floor}(\sigma)} X_{gi}(t) F_{gfi}(t) + \sum_{i=0}^{n=\text{floor}(\sigma)} r_{bg} N_{gi}(t). \tag{2}$$

Here, the "floor" function rounds off the contact ratio σ to the nearest integer (towards a lower value); J_p and J_g are the polar moments of inertia for the pinion and gear; T_p and T_g are the external and braking torques; $N_{pi}(t)$ and $N_{gi}(t)$ are the normal loads defined as follows:

$$N_{pi}(t) = N_{gi}(t) = k_i(t)[r_{bp} \theta_p(t) - r_{bg} \theta_g(t) + x_p(t) - x_g(t)]$$
$$+ c_i(t)[r_{bp} \dot{\theta}_p(t) - r_{bg} \dot{\theta}_g(t) + \dot{x}_p(t) - \dot{x}_g(t)], \quad i = 0, 1, ..., n = \text{floor}(\sigma), \tag{3}$$
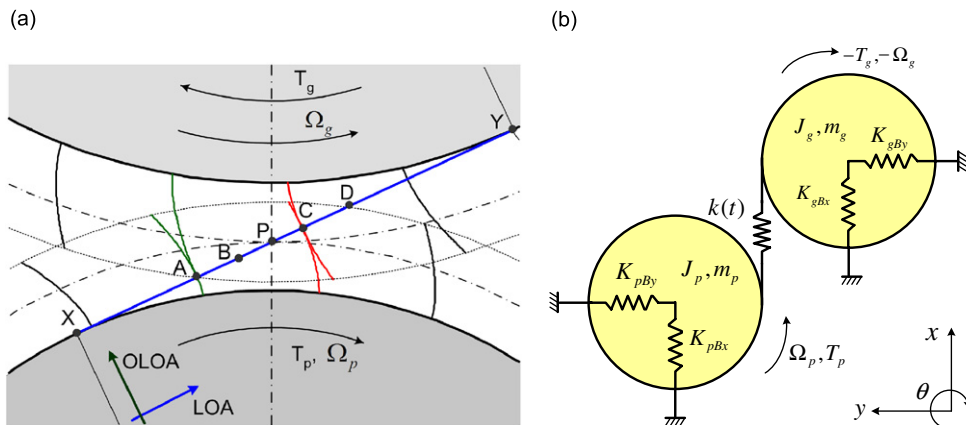

Fig. 1. (a) Snap shot of contact pattern (at $t = 0$) in the spur gear pair; (b) MDOF spur gear pair system; here $k(t)$ is in the LOA direction.

where $k_i(t)$ and $c_i(t)$ are the time-varying realistic mesh stiffness and viscous damping profiles; r_{bp} and r_{bg} are the base radii of the pinion and gear; and $x_p(t)$ and $x_g(t)$ denote the translational displacements (in the LOA direction) at the bearings. The sliding (interfacial) friction forces $F_{pfi}(t)$ and $F_{gfi}(t)$ of the ith meshing pair are derived as follows; note that five alternate $\mu(t)$ models will be described in Section 3:

$$F_{pfi}(t) = \mu(t)N_{pi}(t), \quad F_{gfi}(t) = \mu(t)N_{gi}(t), \quad i = 0,\ldots,n. \tag{4a,b}$$

The frictional moment arms $X_{pi}(t)$ and $X_{gi}(t)$ acting on the ith tooth pair are:

$$X_{pi}(t) = L_{XA} + (n-i)\lambda + mod(\Omega_p r_{bp}t, \lambda), \quad i = 0,\ldots,n, \tag{5a}$$

$$X_{gi}(t) = L_{YC} + i\lambda - mod(\Omega_g r_{bg}t, \lambda), \quad i = 0,\ldots,n. \tag{5b}$$

where "mod" is the modulus function defined as: $mod(x, y) = x - y \, \text{floor}(x/y)$, if $y \neq 0$; "sgn" is the sign function; Ω_p and Ω_g are the nominal operational speeds (in rad/s); and λ is the base pitch. Refer to Fig. 1(a) for length L. The governing equations for the translational motions $x_p(t)$ and $x_g(t)$ in the LOA direction are:

$$m_p\ddot{x}_p(t) + 2\zeta_{pBx}\sqrt{K_{pBx}m_p}\,\dot{x}_p(t) + K_{pBx}x_p(t) + \sum_{i=0}^{n=\text{floor}(\sigma)} N_{pi}(t) = 0, \tag{6}$$

$$m_g\ddot{x}_g(t) + 2\zeta_{gBx}\sqrt{K_{gBx}m_g}\,\dot{x}_g(t) + K_{gBx}x_g(t) + \sum_{i=0}^{n=\text{floor}(\sigma)} N_{gi}(t) = 0. \tag{7}$$

Here, m_p and m_g are the masses of the pinion and gear; K_{pBx} and K_{gBx} are the effective shaft-bearing stiffness values in the LOA direction, and ζ_{pBx} and ζ_{gBx} are their damping ratios. Likewise, the governing equations for the translational motions $y_p(t)$ and $y_g(t)$ in the OLOA direction are written as

$$m_p\ddot{y}_p(t) + 2\zeta_{pBy}\sqrt{K_{pBy}m_p}\,\dot{y}_p(t) + K_{pBy}y_p(t) - \sum_{i=0}^{n=\text{floor}(\sigma)} F_{pfi}(t) = 0, \tag{8}$$

$$m_g\ddot{y}_g(t) + 2\zeta_{gBy}\sqrt{K_{gBy}m_g}\,\dot{y}_g(t) + K_{gBy}y_g(t) - \sum_{i=0}^{n=\text{floor}(\sigma)} F_{gfi}(t) = 0. \tag{9}$$

3. Alternate sliding friction models

3.1. Model I: Coulomb model with $\mu(t)$

The Coulomb friction model with time-varying (periodic) coefficient of friction $\mu_{Ci}(t)$ for the ith meshing tooth pair is derived as follows, where μ_{avg} is the magnitude of the time-average:

$$\mu_{Ci}(t) = \mu_{\text{avg}} \, \text{sgn}[mod(\Omega_p r_{bp}t, \lambda) + (n-i)\lambda - L_{AP}], \quad i = 0,\ldots,n. \tag{10}$$

3.2. Model II: Benedict and Kelley model [8,13]

The instantaneous profile radii of curvature (mm) $\rho(t)$ of ith meshing tooth are:

$$\rho_{pi}(t) = L_{XA} + (n-i)\lambda + mod(\Omega_p r_{bp}t, \lambda), \quad \rho_{gi}(t) = L_{XY} - \rho_{pi}(t), \quad i = 0,\ldots,n. \tag{11a,b}$$

The rolling (tangential) velocities $v_r(t)$ (m/s) of ith meshing tooth pair are:

$$v_{rpi}(t) = \frac{\Omega_p \rho_{pi}(t)}{1000}, \quad v_{rgi}(t) = \frac{\Omega_g \rho_{gi}(t)}{1000}, \quad i = 0,\ldots,n. \tag{12a,b}$$

The sliding velocity $v_s(t)$ and the entraining velocity $v_e(t)$ (m/s) of ith meshing tooth pair are:

$$v_{si}(t) = |v_{rpi}(t) - v_{rgi}(t)|, \quad v_{ei}(t) = |v_{rpi}(t) + v_{rgi}(t)|, \quad i = 0,\ldots,n. \tag{13a,b}$$

The unit normal load (N/mm) is $w_n = T_p/(Z r_{wp} \cos \alpha)$, where α is the pressure angle, Z is the face width (mm), T_p is the torque (N mm) and r_{wp} is the operating pitch radius of pinion (mm). Our $\mu(t)$ prediction for the ith meshing tooth pair is based on the Benedict and Kelley model [8], though it is modified to incorporate a reversal in the direction of friction force at the pitch point. Here, $S_{avg} = 0.5(S_{ap} + S_{ag})$ is the averaged surface roughness (μm), and η_M is the dynamic viscosity of the oil entering the gear contact:

$$\mu_{Bi}(t) = \frac{0.0127 \times 1.13}{1.13 - S_{avg}} \log_{10} \left[\frac{29700 w_n}{\eta_M v_{si}(t) v_{ei}^2(t)} \right] \text{sgn}[mod(\Omega_p r_{bp} t, \lambda) + (n - i)\lambda - L_{AP}]. \tag{14}$$

3.3. Model III: formulation suggested by Xu et al. [9,10]

The composite relative radius of curvature $\rho_r(t)$ (mm) of ith meshing tooth pair is

$$\rho_{ri}(t) = \frac{\rho_{pi}(t)\rho_{gi}(t)}{\rho_{pi}(t) + \rho_{gi}(t)}, \quad i = 0, \ldots, n. \tag{15}$$

The effective modulus of elasticity (GPa) of mating surfaces is $E' = 2/[(1 - v_p^2/E_p) + (1 - v_g^2/E_g)]$, where E and v are the Young's modulus and Poisson's ratio, respectively. The maximum Hertzian pressure (GPa) for the ith meshing tooth pair is

$$P_{hi}(t) = \sqrt{\frac{w_n E'}{2000 \pi \rho_{ri}(t)}}. \tag{16}$$

Define the dimensionless slide-to-roll ratio $SR(t)$ and oil entraining velocity $V_e(t)$ (m/s) of ith meshing tooth pair as

$$SR_i(t) = \frac{2v_{si}(t)}{v_{ei}(t)}, \quad V_{ei}(t) \frac{v_{ei}(t)}{2}, \quad i = 0, \ldots, n. \tag{17a,b}$$

The empirical sliding friction expression (for the ith meshing tooth pair), as proposed by Xu et al. [9,10] based on non-Newtonian, thermal EHL theory, is modified in our work to incorporate a reversal in the direction of the friction force at the pitch point as

$$\mu_{Xi}(t) = e^{f(SR_i(t), P_{hi}(t), \eta_M, S_{avg})} P_{hi}^{b_2} |SR_i(t)|^{b_3} V_{ei}^{b_6}(t) \eta_M^{b_7} R_i^{b_8}(t) \, \text{sgn}[mod(\Omega_p r_{bp} t, \lambda) + (n - i)\lambda - L_{AP}],$$
$$f(SR_i(t), P_{hi}(t), \eta_M, S_{avg}) = b_1 + b_4 |SR_i(t)| P_{hi}(t) \log_{10}(\eta_M) + b_5 e^{-|SR_i(t)| P_{hi}(t) \log_{10}(\eta_M)} + b_9 e^{S_{avg}},$$
$$i = 0, \ldots, n. \tag{18a, b}$$

Xu [10] suggests the following empirical coefficients (in consistent units) for the above formula: $b_1 = -8.916465$, $b_2 = 1.03303$, $b_3 = 1.036077$, $b_4 = -0.354068$, $b_5 = 2.812084$, $b_6 = -0.100601$, $b_7 = 0.752755$, $b_8 = -0.390958$ and $b_9 = 0.620305$.

3.4. Model IV: smoothened Coulomb model

Xu [10] conducted a series of friction measurements on a ball-on-disk test machine and measured the $\mu(t)$ values as a function of SR; these results resemble the smoothening function reported by Duan and Singh [12] near the pitch point ($SR = 0$) especially at very low speeds (boundary lubrication conditions). By denoting the periodic displacement of ith meshing tooth pair as $x_i(t) = mod(\Omega_p r_{bp} t, \lambda) + (n - i)\lambda - L_{AP}$, a smoothing function could be used in place of the discontinuous Coulomb friction [4]. The arc-tangent type function is proposed as follows though one could also use other functions [12]:

$$\mu_{Si}(t) = \frac{2\mu_{avg}}{\pi} \arctan[\Phi x_i(t)] + x_i(t) \frac{2\mu_{avg}\sigma}{\pi[1 + \Phi^2 x_i^2(t)]}, \quad i = 0, \ldots, n. \tag{19}$$

In the above, the regularizing factor Φ is adjusted to suit the need of smoothening requirement. A higher value of Φ corresponds to a steeper slope at the pitch point. In our work, $\Phi = 50$ is used for a comparative study (reported in Section 4).

3.5. Model V: composite friction model

Alternate theories (Models I to IV) seem to be applicable over specific operational conditions. This necessitates a judicious selection of an appropriate lubrication regime as indicated by the film parameter, Λ, that is defined as the ratio of minimum lubrication film thickness and composite surface roughness $R_{comp} = \sqrt{R_{rms,g}^2 + R_{rms,p}^2}$ measured with a filter cutoff wave length L_x, where R_{rms} is the rms gear-tooth surface roughness [14]. The film parameter for rotorcraft gears usually lies between 1 and 10. In the mixed lubrication regime the films are sufficiently thin to yield partial asperity contact, while in the EHL regime the lubrication film completely separates the gear surfaces. Accordingly, a composite friction model is proposed as follows:

$$\mu(t) = \begin{cases} \mu_C(t) & \text{simplified Coulomb model, computationally efficient (Model I),} \\ \mu_B(t) & 1 < \Lambda < 4, \text{ mixed lubrication, (Model II),} \\ \mu_X(t) & 4 \leqslant \Lambda < 10, \text{ EHL lubrication, (Model III),} \\ \mu_S(t) & \text{low } \Omega_p, \text{ high } T_p, \Lambda < 1, \text{ boundary lubrication (Model IV).} \end{cases} \tag{20}$$

Application of Models II, III or IV would, of course, depend on the operational and tribological conditions though Model I could be easily utilized for computationally efficient dynamic simulations [4]. Note that the magnitude μ_{avg} of Model I or IV should be determined separately. For instance, the averaged coefficient based on Model II was used in our prior work [4]. Also, the critical Λ value between different lubrication regimes must be carefully chosen. The film thickness calculation employs the following equation developed by Hamrock and Dowson [11,14], based on a large number of numerical solutions that predict the minimum film thickness for two disks in line contact. Here, G is the dimensionless material parameter, W is the load parameter, U is the speed parameter, H is the dimensionless central film thickness and b_H is the semi-width of Hertzian contact band:

$$\Lambda_i(t) = \frac{H_{ci}(t)\rho_{r1}(t) \times 10^3}{R_{comp}} \sqrt{\frac{L_X}{2b_{Hi}(t)}}, \quad i = 0, \ldots, n, \tag{21a}$$

$$b_{H1}(t) = \sqrt{\frac{8w_n\rho_{r1}(t)}{\pi E_r}}, \quad H_{ci}(t) = 3.06\frac{G^{0.56}U_i^{0.69}(t)}{W_i^{0.10}(t)}, \quad G = k\eta_M^s E_r, \tag{21b,c}$$

$$U_i(t) = \frac{\eta_M v_{ei}(t)}{2E_r\rho_{ri}(t)} \times 10^{-6}, \quad W_i(t) = \frac{w_n}{E_r\rho_{ri}(t)}. \tag{21d,e}$$

4. Comparison of sliding friction models

In Fig. 2(a) are shown the magnitudes of $\mu(t)$ as predicted by Models II and III for a spur gear set [4] given $T_p = 22.6$ N m (200 lb in) and $\Omega_p = 1000$ rev/min. The linear time-varying formulations for meshing tooth pairs #0 and #1 result in periodic profiles for both models. Two major differences between these two models are: (1) the averaged magnitude from Model II is much higher compared with that of Model III since friction under mixed lubrication is generally higher than under EHL and (2) while Model III predicts nearly zero friction near the pitch point, Model II predicts the largest μ value due to the entraining velocity term in the denominator. As explained by Xu [10], three different regions could be roughly defined on a μ versus SR curve. When the sliding velocity is zero, there is no sliding friction, and only rolling friction (though very small) exists. Thus, the μ value should be almost zero at the pitch point. When the SR is increased from zero, μ first increases linearly with small values of SR. This region is defined as the linear or isothermal region. When the SR is increased slightly further, μ reaches a maximum value and then decreases as the SR value is increased beyond that point. This region is referred to as nonlinear or non-Newtonian region. As the SR is increased further, the friction decreases in an almost linear fashion; this is called as the thermal region. Model II seems to be valid only in the thermal region [9,10].
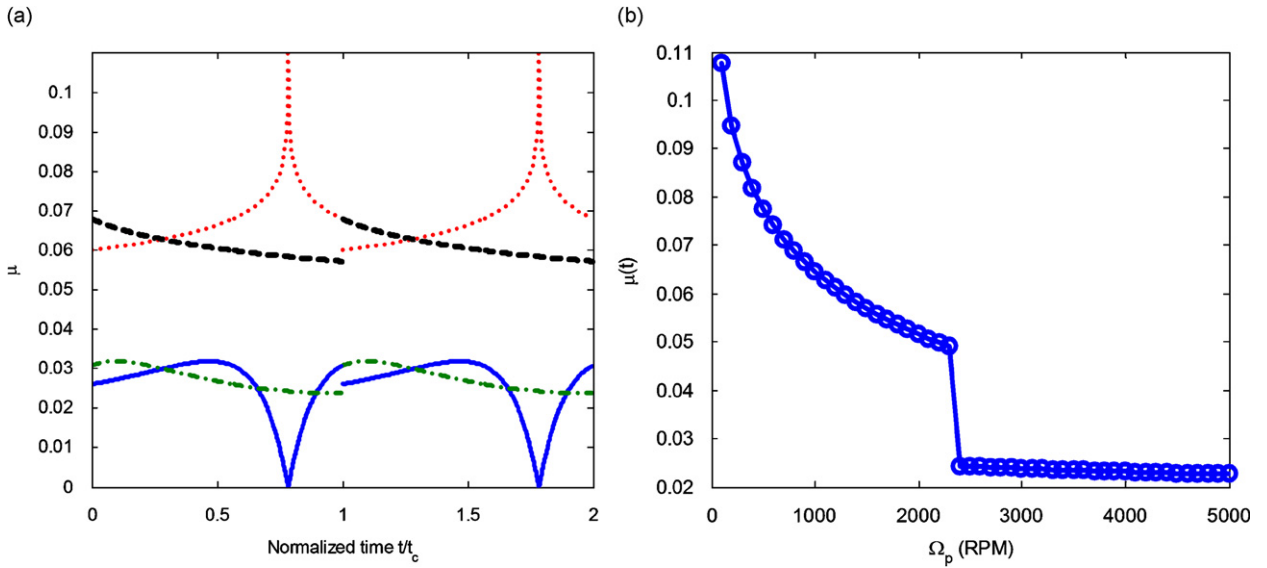
(a)

(b)

Fig. 2. (a) Comparison of Model II [8] and Model III [9] given $T_p = 22.6$ N m (200 lb in) and $\Omega_p = 1000$ rev/min. Key: ▪▪▪▪▪ pair #1 with Model II; ▬ ▬ pair #0 with Model II; ▬▬▬ pair #1 with Model III; ▬ ▪ ▬ pair #0 with Model III; (b) Averaged magnitude of the coefficient of friction predicted as a function of speed using the composite Model V with $T_p = 22.6$ N m (200 lb in). Here, t_c is one mesh cycle.
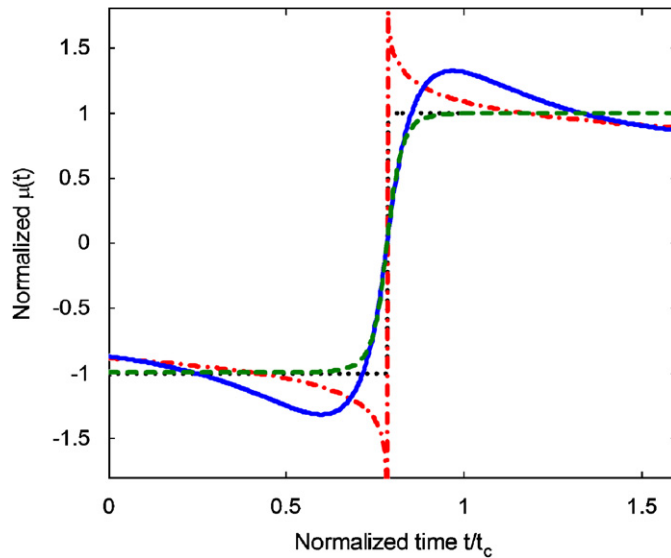

Fig. 3. Comparison of normalized friction models. Key: ▪▪▪▪▪ Model I (Coulomb friction with discontinuity); ▬ ▪ ▬ Model II [8]; ▬▬▬ Model III [9]; ▬ ▬ Model IV (smoothened Coulomb friction). Note that curve between $0 \leqslant t/t_c < 1$ is for pair #1; and the curve between $1 \leqslant t/t_c < \sigma$ is for pair #0.

Fig. 2(b) shows the averaged magnitude of μ_{avg} predicted as a function of Ω_p using the composite formulation (Model V) with $T_p = 22.6$ N m (200 lb in). An abrupt change in magnitude is found around 2500 rev/min corresponding to a transition from the EHL to a mixed lubrication regime. Similar results could be obtained by plotting the composite $\mu(t)$ as a function of T_p. Though our composite model could be used to predict $\mu(t)$ over a large range of lubrication conditions, care must be exercised since the calculation of Λ itself is based on an empirical equation [11].

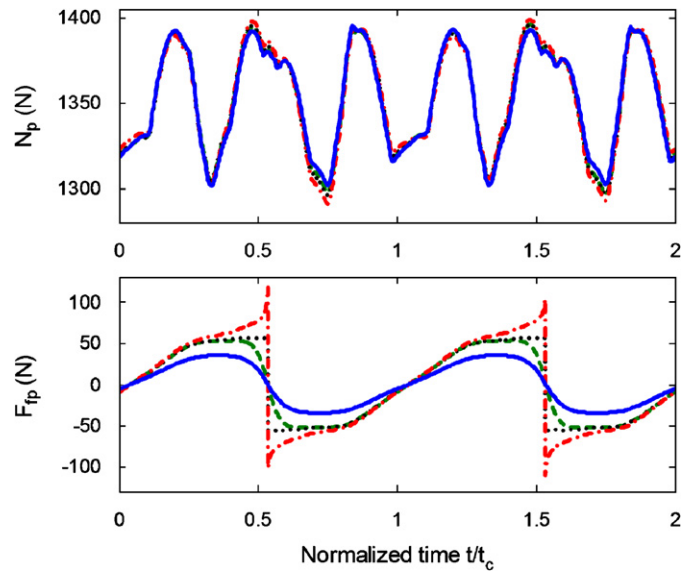Fig. 4. Combined normal load and friction force time histories as predicted using alternate friction models given $T_p = 56.5\,\mathrm{N\,m}$ (500 lb in) and $\Omega_p = 4875\,\mathrm{rev/min}$. Key: ▪▪▪▪▪▪ Model I; ▬ · ▬ Model II; ▬▬▬ Model III; ▬ ▬ Model IV.
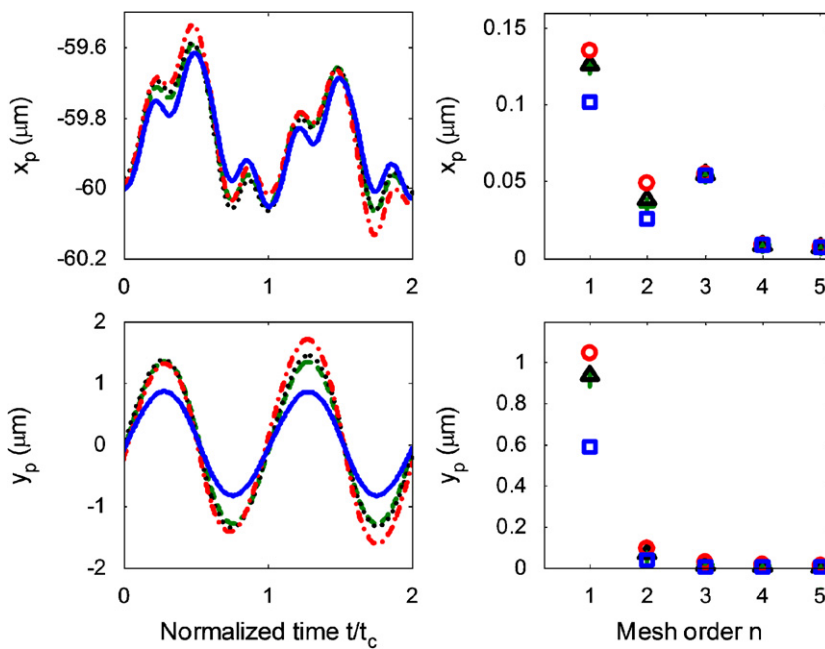

Fig. 5. Predicted line-of-action and off-line-of-action displacements using alternate friction models given $T_p = 56.5\,\mathrm{N\,m}$ (500 lb in) and $\Omega_P = 4875\,\mathrm{rev/min}$. Key: in time domain: ▪▪▪▪▪▪ Model I; ▬ · ▬ Model II; ▬▬▬ Model III; ▬ ▬ Model IV; in frequency (mesh order n) domain: △ Model I; ◯ Model II; ☐ Model III; + Model IV.

Fig. 3 compares four friction models on a normalized basis. The curves between $0 \leqslant t/t_c < 1$ are defined for pair ♯1 and those between $1 \leqslant t/t_c < \sigma$ are defined for pair ♯0. Discontinuities exist near the pitch point for Models I and II, and these might serve as artificial excitations to the OLOA dynamics. On the other hand, smooth transitions are observed for Models III and IV corresponding to the EHL condition. Fig. 4 compares the combined normal loads and friction force time histories as predicted by four friction models given $T_p = 56.5\,\mathrm{N\,m}$ (500 lb in) and $\Omega_p = 4875\,\mathrm{rev/min}$. Note that while Fig. 3 illustrates $\mu(t)$ for each meshing tooth

pair the friction forces of Fig. 4 include the contributions from both (all) meshing tooth pairs. Though alternate friction formulations dictate the dynamic friction force profiles, they have negligible effect on the normal loads.

5. Validation and conclusion

Fig. 5 compares the predicted LOA and OLOA displacements with alternate friction models given $T_p = 56.5\,\mathrm{N\,m}$ (500 lb in) and $\Omega_p = 4875\,\mathrm{rev/min}$. Note that the differences between predicted motions are not
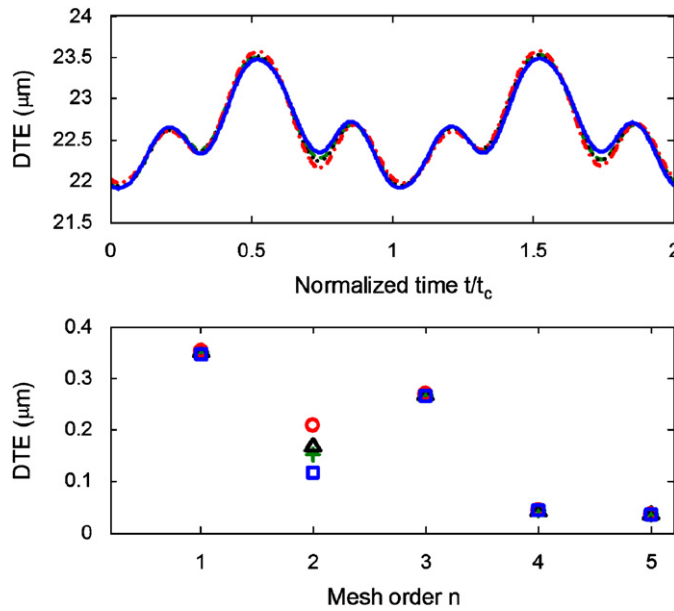

Fig. 6. Predicted dynamic transmission error (DTE) using alternate friction models given $T_p = 56.5\,\mathrm{N\,m}$ (500 lb in) and $\Omega_p = 4875\,\mathrm{rev/min}$. Key: in time domain: ▪▪▪▪▪▪ Model I; ▬ · ▬ Model II; ▬▬▬ Model III; ▬ ▬ Model IV; in frequency (mesh order n) domain: △ Model I; ○ Model II; □ Model III; + Model IV.
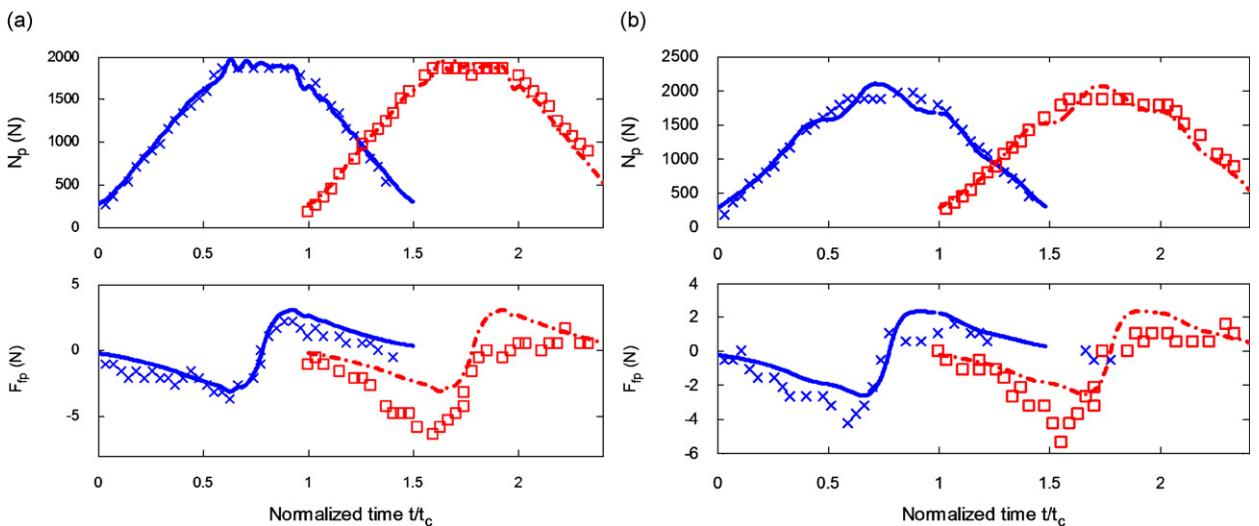

Fig. 7. Validation of the normal load and sliding friction force predictions: (a) at $T_p = 79.1\,\mathrm{N\,m}$ (700 lb in) and $\Omega_p = 800\,\mathrm{rev/min}$; (b) at $T_p = 79.1\,\mathrm{N\,m}$ (700 lb in) and $\Omega_p = 4000\,\mathrm{rev/min}$. Key: ▬▬▬ prediction of tooth pair A with Model III; ▬ · ▬ prediction of tooth pair B with Model III; ✕ measurement of tooth pair A [13]; □ measurement of tooth pair B [13].

significant though friction formulations and friction force excitations differ. This implies that one could still employ the simplified Coulomb formulation (Model I) in place of more realistic time-varying friction models (Models II to IV). Similar trend is observed in Fig. 6 for the dynamic transmission errors (DTE), defined as $\delta(t) = r_{bp}\theta_p(t) - r_{bg}\theta_g(t) + x_p(t) - x_g(t)$. The most significant variation induced by friction formulation is at the second harmonic, which matches the results reported by Lundvall et al. [7].

Finally, predicted normal load and friction force time histories (with Model III) are validated using the benchmark friction measurements made by Rebbechi et al. [13]. Results are shown in Fig. 7. Based on the comparison, μ is found to be about 0.004 since it was not given in the experimental study. Here, we have made the periodic LTV definitions of meshing tooth pairs ♯0 and ♯1 to be consistent with those of measurements, where meshing tooth pairs A and B are labeled in a continuous manner. Predictions match well with measurements at both low ($\Omega_p = 800$ rev/min) and high ($\Omega_p = 4000$ rev/min) speeds. Ongoing research focuses on the development of semi-analytical solutions given a specific $\mu(t)$ model and an examination of the interactions between tooth modifications and sliding friction.

Acknowledgments

References

[1] M. Vaishya, R. Singh, Analysis of periodically varying gear mesh systems with Coulomb friction using Floquet theory, *Journal of Sound and Vibration* 243 (3) (2001) 525–545.

[2] M. Vaishya, R. Singh, Sliding friction-induced non-linearity and parametric effects in gear dynamics, *Journal of Sound and Vibration* 248 (4) (2001) 671–694.

[3] M. Vaishya, R. Singh, Strategies for modeling friction in gear dynamics, *ASME Journal of Mechanical Design* 125 (2003) 383–393.

[4] S. He, R. Gunda, R. Singh, Effect of sliding friction on the dynamics of spur gear pair with realistic time-varying stiffness, *Journal of Sound and Vibration* 301 (3–5) (2007) 927–949.

[5] P. Velex, V. Cahouet, Experimental and numerical investigations on the influence of tooth friction in spur and helical gear dynamics, *ASME Journal of Mechanical Design* 122 (4) (2000) 515–522.

[6] P. Velex, P. Sainsot, An analytical study of tooth friction excitations in spur and helical hears, *Mechanism and Machine Theory* 37 (2002) 641–658.

[7] O. Lundvall, N. Strömberg, A. Klarbring, A flexible multi-body approach for frictional contact in spur gears, *Journal of Sound and Vibration* 278 (3) (2004) 479–499.

[8] G.H. Benedict, B.W. Kelley, Instantaneous coefficients of gear tooth friction, *Transactions of the American Society of Lubrication Engineers* 4 (1961) 59–70.

[9] H. Xu, A. Kahraman, N.E. Anderson, D.G. Maddock, Prediction of mechanical efficiency of parallel-axis gear pairs, *ASME Journal of Mechanical Design* 129 (1) (2007) 58–68.

[10] H. Xu, Development of a generalized mechanical efficiency prediction methodology, PhD Dissertation (Advisor: A. Kahraman), The Ohio State University, 2005.

[11] B.J. Hamrock, D. Dowson, Isothermal elastohydrodynamic lubrication of point contacts, part III—fully flooded results, *Journal of Lubrication Technology* 99 (2) (1977) 264–276.

[12] C. Duan, R. Singh, Dynamics of a 3DOF torsional system with a dry friction controlled path, *Journal of Sound and Vibration* 289 (4–5) (2006) 657–688.

[13] B. Rebbechi, F.B. Oswald, D.P. Townsend, Measurement of gear tooth dynamic friction, *ASME Power Transmission and Gearing Conference Proceedings*, San Diego, 6–9 October 1996, DE-Vol. 88, pp. 355–363.

[14] AGMA Information Sheet 925-A03, Effect of lubrication on gear surface distress, 2003.